8th International Conference
on
Wind Turbine Noise
Lisbon – 12th to 14th May 2019

Aeroacoustic Optimization of a Small Wind Turbine - Methodology and Experimental Validation

K. Volkmer, N. Kaufmann, T. Carolus
University of Siegen, 57076 Siegen, Germany

Corresponding author: kevin.volkmer@uni-siegen.de

Summary

Overall objective of the work presented is the aeroacoustic optimization of an existing small 3 m-diameter horizontal axis wind turbine, equipped with blades made of NREL's S83x airfoil sections. In this work, an acoustically improved airfoil shape was developed via a KAMRUZZAMAN/AMIET trailing edge noise prediction model that is integrated into an evolutionary algorithm. The acoustic and aerodynamic performance of both, the baseline and optimized airfoil segment, were validated experimentally in an aero-acoustic wind tunnel. In a second step new turbine blades were designed with the blade-element-momentum design method utilizing the new airfoil shape. A set of new blades was manufactured. The baseline and modified turbine were tested in a realistic free field environment, requiring statistical methods for the evaluation of power and sound data. The control of the turbine is such that in average it operates at design tip speed ratio (λ = 7.5). Off-design points are not considered in this study.

The aerodynamic noise of the wind turbine with the new optimized blades could be reduced by up to 4 dB in the frequency range from 1 to 6 kHz. The penalty is an increase of high frequency noise at around 7.5 kHz. This modification of the turbine's noise signature is clearly audible close to the turbine. In the distance of less than 100 m a listener does not perceive the high frequency component and experiences a substantial reduction of the perceived turbine noise. The overall aerodynamic performance of the new blades is equivalent or even slightly better as compared to the baseline.

Nomenclature

Symbols

$B_{1,2,3}$ = parameters in KAMRUZZAMAN model
C = chord length
C_d = section drag coefficient (for a two-dimensional airfoil)
C_f = skin friction coefficient (for a two-dimensional airfoil)
C_l = section lift coefficient
F = force per meter of airfoil section span
H = boundary layer shape factor
I = radiation integral
K = convective wavenumber
L = span
L_{Spp} = level of power spectral density of far field acoustic pressure
M = free stream Mach number
$OSPL$ = overall sound pressure level
$\overline{\overline{OSPL}}$ = spatial chordwise and angle of attack averaged overall far field sound pressure level
P = power
PT = penalty term
R_T = ratio of outer to inner boundary layer timescale
S_O = corrected observer distance
S_{pp} = power spectral density of far field acoustic pressure
St = Strouhal number
TI = turbulent intensity of ingested flow
U_c = convection velocity
c = wind speed
c_s = speed of sound
f = frequency
f_{obj} = objective function
f_{peak} = noise peak frequency
g = weighting factor
h = trailing edge thickness
k = acoustic wavenumber
l_y = spanwise correlation length
ls = length scale for BROOKS-POPE-MARCOLINI-model
m = number of design angles of attack
n = number of chordwise positions for wall pressure fluctuation predictions
n_{PT} = number of penalty terms
$ncrit$ = critical N-factor in XFoil
$nfft$ = number of discrete Fourier points
p = pressure
p,q = exponents in KAMRUZZAMAN model
u_τ = skin friction velocity
w = flow velocity
$x_{1,2,3}$ = Cartesian co-ordinates

Greek symbols

Φ_{pp} = power spectral density of surface pressure fluctuations

Π_c = COLE's wake strength parameter
α = effective angle of attack
β_c = CLAUSER's equilibrium parameter
δ^* = boundary layer displacement thickness
ε = lift-to-drag-ratio
θ = boundary layer momentum thickness
κ = frequency parameter
λ = tip speed ratio
ν = kinematic viscosity
ρ = air density
σ = standard deviation of wind speed
τ_w = wall shear stress
ω = angular frequency
ξ = chordwise airfoil coordinate starting at the leading edge

Subscripts
Spp = power spectral density of far field acoustic pressure
l = lift
d = drag
e = position at boundary layer edge
eff = effective
obj = objective
peak = noise peak
ref = reference
w = weighing
∞ = in free stream / at position far upstream

Abbreviations
BG = background
BPM = BROOKS-POPE-MARCOLINI
Exp. = experiment
Mic. = microphone
Pred. = prediction
TE = trailing edge

1. Introduction

Several targets are relevant for designing the twisted, tapered and carefully profiled blades of horizontal axis wind turbines. Naturally, the maximum energy output of a wind turbine is of primary concern and achieved by optimal aerodynamic design. Yet, mitigation of flow induced noise is on a par with efficiency, structural durability, cost, etc.

Overall objective of the work presented is the aeroacoustic optimization of an existing small 3 m-diameter horizontal axis wind turbine. This baseline wind turbine (design inflow velocity c_0 = 6 m/s, design tip speed ratio λ = 7.5) was designed via the classical GLAUERT/SCHMITZ blade-element-momentum method (see e.g. GERHARD et al. [1]). The blades were made of NREL's S83x airfoil sections which were designed as "a family of quiet, thick, natural-laminar-flow airfoils for 1 to 3 m-diameter

turbines" (SOMERS [2]). In particular, the outward part of the blades is made from S834 airfoils with a thickness/chord ratio of 15 %. The baseline turbine has been operated for many years on the roof of a building at the University of Siegen, equipped with a large number of sensors, among those two stationary and turbine mounted weatherproof microphones and a phased microphone array, see appendix A. A prestudy (appendix B) confirmed that the main region of sound radiation is the outward part of the blade (but not the blade tip). This and the fact that the flow velocity around the blade unavoidably increases towards the tip led to the hypothesis that trailing edge (TE) noise is the dominant noise source. TE noise is caused by pressure fluctuations on the blade surfaces due to the turbulent boundary layer which develops in streamwise direction on the blade surfaces. The pressure fluctuations are scattered when convected past the trailing edge. Thus, details of the turbulent flow around each airfoil shaped blade section and - causally connected - the airfoil geometry itself becomes relevant.

Different techniques for trailing edge (TE) noise mitigation are currently under investigation or even state-of-the-art. State-of-the-art are rigid serrated trailing edges (HOWE [3] and GRUBER [4]), recently refined towards flexible serrations (KLEMME and CHRISTOPH [5]). Other research deals with blowing or sucking air through small slots at the blade surface for manipulating the boundary layer in the TE region (GERHARD [6] and WOLF et al. [7]). The design of per se low-noise airfoil shapes and their effect on the overall turbine noise emission has been tackled by wind turbine aerodynamicists but - to the knowledge of the authors - not much has been published (see e.g. LUTZ et al. [8]), OERLEMANS et al. [9]).

In this work, an acoustically improved airfoil shape is developed via a model-based optimization scheme. In a second step new turbine blades are designed utilizing the new airfoil shape while keeping all other design parameters of the turbine constant. A 2D airfoil segment and a set of new blades were manufactured. Eventually, both, an airfoil segment with the new profile and the complete turbine are investigated experimentally in an aero-acoustic wind tunnel and in situ for validation of the predicted noise reduction.

2. Methodology for airfoil shape optimization

Fig. 1 shows the structure of the airfoil optimization scheme developed. Core is a semi-analytical airfoil trailing edge sound prediction model. Boundary layer parameters, that are essential inputs into the acoustic model as well as the overall aerodynamic airfoil performance data (lift and drag as a function of angle of attack, i.e the polars), are determined by a panel method. Everything is integrated into an optimization loop, here an evolutionary algorithm. The result is an airfoil shape which should be optimal with respect to TE noise.

Advanced semi-analytical acoustic prediction schemes follow a two step procedure: Firstly, the prediction of the wall pressure fluctuations beneath the turbulent boundary layer and, secondly, the modeling of the scattering of these fluctuations at the trailing edge and the generation of sound. For the scattering at the trailing edge AMIET's far field noise model [10], extended by ROGER and MOREAU [11], is utilized in this work. The prediction of the wall pressure fluctuations is more challenging and much research has been undertaken in the recent years (see e.g. ROZENBERG et al. [12], CATLETT et al. [13, 14], HU and HERR [15], KAMRUZZAMAN et al. [16]).

Motivated by a comparative study by LEE and VILLAESCUSA [17] the model by KAMRUZZAMAN et al. [16] (in the following abbreviated as "KAMRUZZAMAN model") is employed.

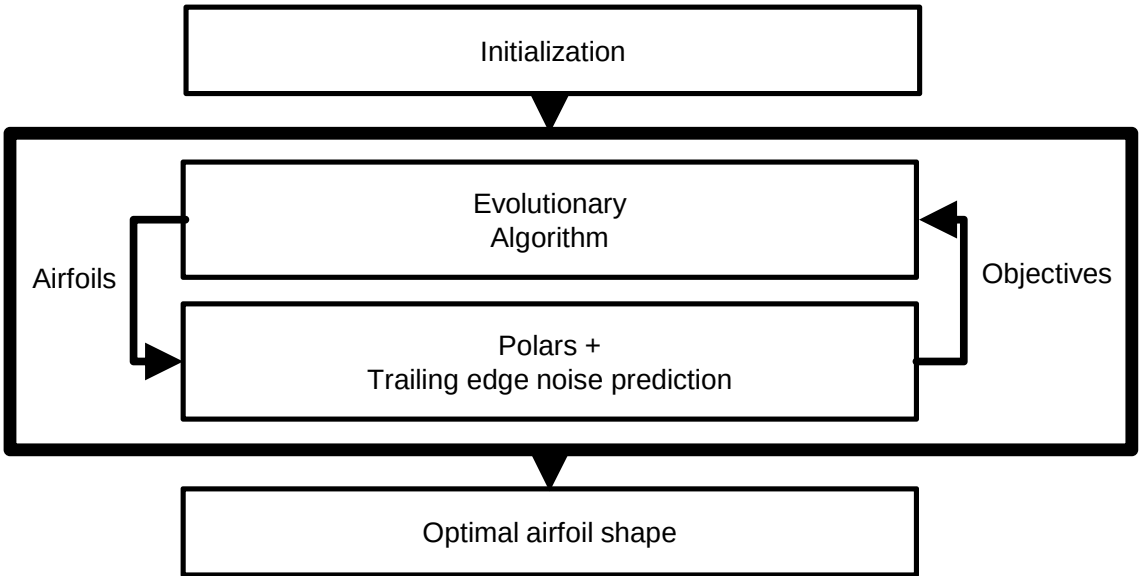

Fig. 1: Flow chart of airfoil shape optimization

2.1 KAMRUZZAMAN's wall pressure model

The KAMRUZZAMAN model [16] yields the wall pressure fluctuations Φ_{pp} in a single sided spectral formulation at a given chordwise position of the airfoil:

$$\frac{\Phi_{pp}(\omega) w_e}{\tau_w^2 \delta^*} = \frac{B_2 \cdot \left(\frac{\omega\delta^*}{w_e}\right)^2}{\left[\left(\frac{\omega\delta^*}{w_e}\right)^p + B_1\right]^q + \left[B_3\left(\frac{\omega\delta^*}{w_e}\right)\right]^7} \tag{1}$$

w_e is the velocity at the edge of the boundary layer, τ_w is the wall shear stress, δ^* the displacement thickness, $\omega = 2\pi f$ the angular frequency, B_1 = 0.27, B_3 = 1.15 $R_T^{-2/7}$, p = 1.637, q = 2.47,

$$R_T = \frac{\delta^* u_\tau^2}{w_e \nu} \tag{2}$$

with u_τ being the skin friction velocity and ν the kinematic viscosity, and

$$B_2 = 0.45\left[1.75\left(\Pi_c^2 \beta_c^2\right)^m + 15\right] \text{ with } m = 0.5\left(\frac{H}{1.31}\right)^{0.3}. \tag{3}$$

$H = \delta^*/\theta$ is the boundary layer shape factor with θ being the boundary layer momentum thickness. β_c is CLAUSER's parameter and in the KAMRUZZAMAN model calculated as

$$\beta_c = \left(\frac{1.7 + \sqrt{2/C_f}\,(1 - 1/H)}{6.1} \right)^2 - 1.81, \tag{4}$$

where C_f is the skin friction coefficient. The free stream pressure gradient is

$$\Pi_c = 0.277, \text{ if } \beta_c \leq -0.5,$$

and otherwise

$$\Pi_c = 0.8\left(\beta_c + 0.5\right)^{0.75}. \tag{5}$$

It is worth to note that, as in other recent wall pressure spectral models, inputs are local boundary layer parameters like the velocity at the boundary layer edge as well as parameters which take into account the upstream history of the boundary layer like the boundary layer displacement thickness (cp. ROZENBERG et al. [12]).

2.2 AMIET's trailing edge noise model

The computed wall pressure spectrum serves as an input into AMIET's trailing edge far field noise model [10]. The trailing edge is equivalent to the x_2-axis in spanwise direction, Fig. 2; x_1 is the chordwise coordinate and x_3 the direction perpendicular to the airfoil surface; the origin of the coordinate system is at mid span. The chord length of the airfoil is C, its span L, the flow angle of attack α and the free stream flow velocity w_∞ are also denoted. Additionally, a coordinate ξ is introduced as a chordwise airfoil coordinate starting at the leading edge.

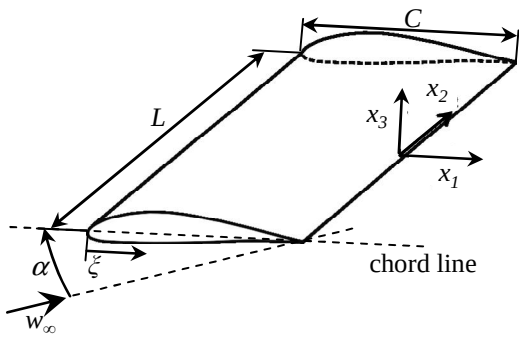

Fig. 2: Airfoil section and co-ordinate system; origin at mid span at the trailing edge

ROGER and MOREAU [11] added back scattering at the leading edge and a 3D extension to AMIET's original model [10]. The 3D extension is required for predictions at oblique observer positions with non-zero x_2-components. The first extension is utilized, whereas the second is implemented but not used as no oblique observer positions occur in the context of this work. The simplified model for large aspect ratios L/C is used. The spectral density of the acoustic far field sound pressure is

$$S_{pp}(\boldsymbol{x},\omega)=\left(\frac{x_3}{S_0^2}\right)^2\left(\frac{\omega C}{4\pi c_s}\right)^2 2\pi L\left|I\left(\frac{K}{C},\frac{kx_2}{CS_0},\kappa\right)\right|^2\frac{1}{\pi}\Phi_{pp}l_{x2} \tag{6}$$

with the speed of sound c_s, the observer distance, corrected for convection effects,

$$S_0=\sqrt{x_1^2+\left(1-M^2\right)\left(x_2^2+x_3^2\right)}, \tag{7}$$

the wall pressure spectrum Φ_{pp} and the spanwise correlation length l_y. The spanwise correlation length l_y is calculated as in TIAN et al. [18] with the help of the CORCOS model [19]. The airfoil response function I is - among others - a function of the acoustic wave number $k = \omega/c_s$ and the convective wave number $K = \omega/U_c$ with U_c being the convection velocity. Details about the airfoil response function can be found in [11]. Also super- and subcritical gusts are included which occur for $\kappa_2 > 0$ and $\kappa_2 < 0$, respectively, where

$$\kappa^2=\left(\frac{KM}{1-M^2}\right)^2-\frac{K_2^2}{1-M^2} \tag{8}$$

and the free stream Mach number $M = w_\infty/c_s$. As the large aspect ratio assumption is applied, the aerodynamic wave number in spanwise direction is $K_2 = kx_2/S_0$.

Note that a modification of the 2D airfoil shape (keeping all other dimensions of the airfoil section constant) will affect the wall pressure fluctuations only. Hence, minimizing trailing edge noise basically reduces to minimizing the near trailing edge wall pressure fluctuations. AMIET's acoustic model simply "transfers" these fluctuations into the acoustic far field.

2.3 Aerodynamic airfoil performance

A panel method as implemented in *XFOIL* by DRELA [20] is used to determine all overall airfoil performance parameters like pressure distribution, lift and drag, but also the boundary layer parameters. The section lift coefficient C_l is calculated by the lift force per unit length of airfoil section span F_l (for an infinite wing) and the section drag coefficient with the drag force per unit length of airfoil section span F_d (for an infinite wing) acting on a reference chord length C_{ref} = 1 m

$$C_l\equiv\frac{F_l}{0.5\rho w_\infty^2 C_{ref}} \tag{9}$$

$$C_d\equiv\frac{F_d}{0.5\rho w_\infty^2 C_{ref}} \tag{10}$$

with the free stream velocity w_∞ and the fluid density ρ. The lift to drag ratio is calculated as

$$\varepsilon\equiv\frac{C_l}{C_d}. \tag{11}$$

The boundary layer parameters are normalized with the chord length (as the boundary layer displacement thickness δ^* and momentum thicknesses θ) or with the inflow velocity (as the velocity at the boundary layer edge w_e).

2.4 Optimization scheme

The airfoil geometry, i.e. the shape of pressure and suction side, is parameterized via Bezier curves as in KAUFMANN [21].

An evolutionary algorithm is applied, since - in contrast to e.g. gradient based schemes - it is able to find the global optimum. It is described by BAMBERGER [22], who was inspired by the textbook from THÉVENIN and JANIGA [23].

The objective function is set as

$$f_{obj}\left(\boldsymbol{x}_{Bez}\right) = -\overline{\overline{OSPL}}_{obj} - \sum_{i}^{n_{PT}} g_i PT_i \,. \qquad \textbf{(12)}$$

$\overline{\overline{OSPL}}_{obj}$ is an overall sound pressure level averaged over a) the range of design angles of attack[1], b) several chordwise positions (for evaluation of wall pressure spectra) per angle of attack (see appendix D). This type of averaging ensures a non-local optimization. PT_i are n_{PT} penalty terms which are weighted by weighing factors g_i. The penalty terms are formulated such that

1. the thickness of the airfoil increases monotonically from leading edge to the maximum thickness and then decreases monotonically towards the trailing edge of the airfoil
2. extremely thin airfoils close to the trailing edge are avoided
3. separation is excluded all along the chord for the targeted angle of attack by sorting out airfoil shapes associated with boundary layer shape factors larger than 2.5 which is inspired by CLAUSER [25]
4. a decrease of lift below a set limit is avoided

Since the primary target of this work is a low noise airfoil, neither a restriction for the maximum airfoil thickness (often necessary for structural reasons) is implemented nor is the lift-to-drag ratio considered in the objective function.

The population size in the evolutionary algorithm is 150 individuals. Crossover between the parent parameters, i.e. Bezier points, followed by mutation is applied to produce the individuals of the next generation. The mutation range producing the following generation is confined to a percentage of the difference between the lowest and highest magnitude of the respective parameter in the previous generation. This percentage is 90% in the first 40 generations and 40% after. Only the best individual, the elite, will survive and be transferred to the next generation. Crossover is only performed within the first 40 generations. Convergence is reached if the Bezier points of the best individual vary less than 0.1% of the difference of the initial parameter limits within the last 40 generations.

[1] A turbine blade of a fixed pitch, variable speed turbine operates in a relatively small range of angles of attack (variations are mainly caused by atmospheric gusts and turbulences, GIGUERE and SELIG [24]). Hence, here the range of angles of attack is limited to α = 2° - 6°.

3. Results

3.1 Airfoil

The typical value of the Reynolds number for this small-wind-turbine application is in the order of 200,000. Nevertheless, blade surface roughness due to operation in the real world and atmospheric free stream turbulence may cause a fully turbulent flow around the turbine blades and hence the airfoil segments (see eg. MCAULIFFE et al. [26]). Therefore, as the worst case scenario, the airfoil segment is optimized assuming of a fully turbulent boundary layer along pressure and suction side. To mimic a fully turbulent flow, tripping is applied at 2% and 5% of the airfoil section of chord length *C* on the suction and pressure side, respectively.

The geometries of the baseline airfoil and the obtained optimized airfoil KV200 are depicted in Tab. 1. It can be seen that the resulting maximum thickness of the KV200 is less than the one of the baseline profile, as the optimizer had the freedom to vary the thickness. The polars of lift, lift-to-drag-ratio as predicted from *XFOIL* and the far field sound from the combined KAMRUZZAMAN/AMIET/XFOIL trailing edge sound model are presented in Fig. 3. As compared to the S834 the lift polar of the new KV200 is similar whereas the lift-to-drag-ratio of the KV200 has even improved (although not included in the optimization objectives). One has to keep in mind that for the baseline and optimized airfoils - as stated earlier - tripping was applied very close to the leading edge in order to mimic a fully turbulent boundary layer. Of course, a S834 airfoil with natural transition would have a substantially better lift-to-drag-ratio. The far field sound pressure level *OSPL* was predicted based on the wall pressure fluctuations at $\xi = 0.98\ C$ and again the far field contributions of pressure and suction side are added. (This is different from the objective function that was based on the average of wall pressure spectra at different chordwise positions for a range of angle of attacks.) As the angle of attack is increased, the *OSPL* values of both airfoils increase as well. At the chosen chordwise position *XFOIL* predicts local flow separation on the suction side of the S834 close to an angle of attack of 6° and, hence, the KAMRUZZAMAN model [16] is not applicable anymore. This is already noticeable by the sharp drop of the *OSPL* values of the S834 in the lower diagram in Fig. 3 close to that angle. Surprisingly, the predicted *OSPL* of the optimized airfoil KV200 is up to 10 dB lower as compared to the baseline airfoil.

Tab. 1: Baseline and optimized airfoil

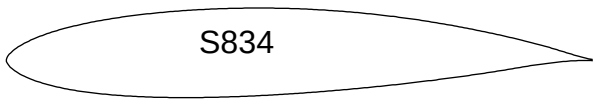	Baseline airfoil
	Optimized for low far field noise

The baseline airfoil S834 and the optimized airfoil KV200 are also investigated experimentally in a small aeroacoustic wind tunnel as in appendix C. In order to perform a fair comparison both airfoils are compared at a same lift coefficient. Two different values of the lift coefficient, C_L = 0.38 and 0.64 are chosen for validation. In order to compensate for wind tunnel effects the geometrical angle of attack is set such that the static pressure distributions from the experiment and *XFOIL* agree.

The experimental results depicted in Fig. 4 deviate considerably from the predicted. Nevertheless, they demonstrate that the far field sound emitted by the optimized airfoil KV200 is reduced in the low frequency range of approx. 100 to 600 Hz by up to 4 dB as compared to the baseline S834. The BROOKS-POPE-MARCOLINI (BPM)-model [27] supports trailing edge noise to be expected at this frequency range (see appendix E). At medium frequencies a slight increase of noise is present for the optimized KV200 and the higher lift configuration. The experimental data in the high frequency range are irrelevant, since they are hidden in the empty wind tunnel background noise.

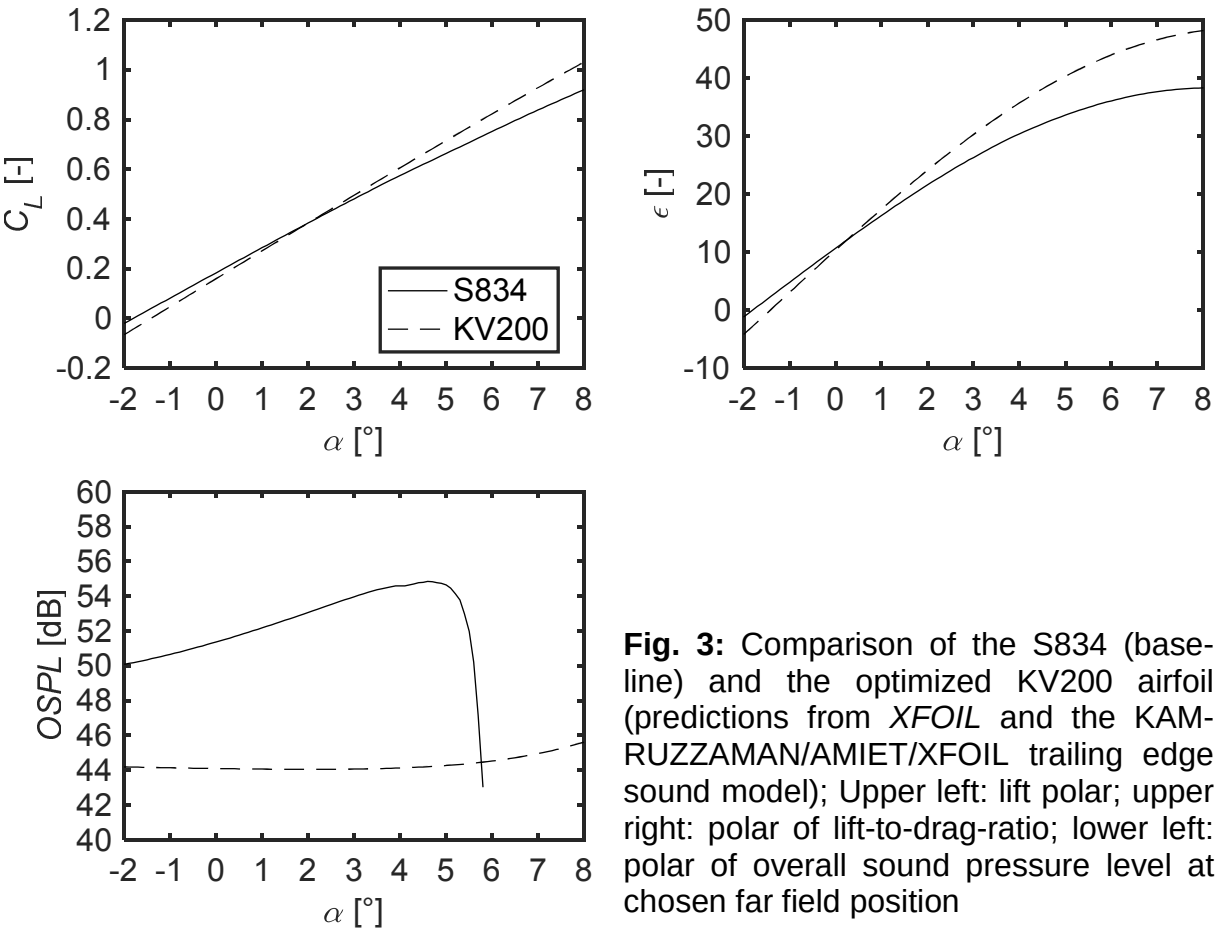

Fig. 3: Comparison of the S834 (baseline) and the optimized KV200 airfoil (predictions from *XFOIL* and the KAMRUZZAMAN/AMIET/XFOIL trailing edge sound model); Upper left: lift polar; upper right: polar of lift-to-drag-ratio; lower left: polar of overall sound pressure level at chosen far field position

3.2 Blade

Employing the acoustically optimized KV200 airfoil new blades B-KV200 for replacing the baseline blades are designed. Given the similar lift polars of the KV200 and the S834, the main blade parameters such as the spanwise distribution of chord length and pitch angle could have kept equal or similar. Fig. 5 shows the contour of the new blade and some section views.

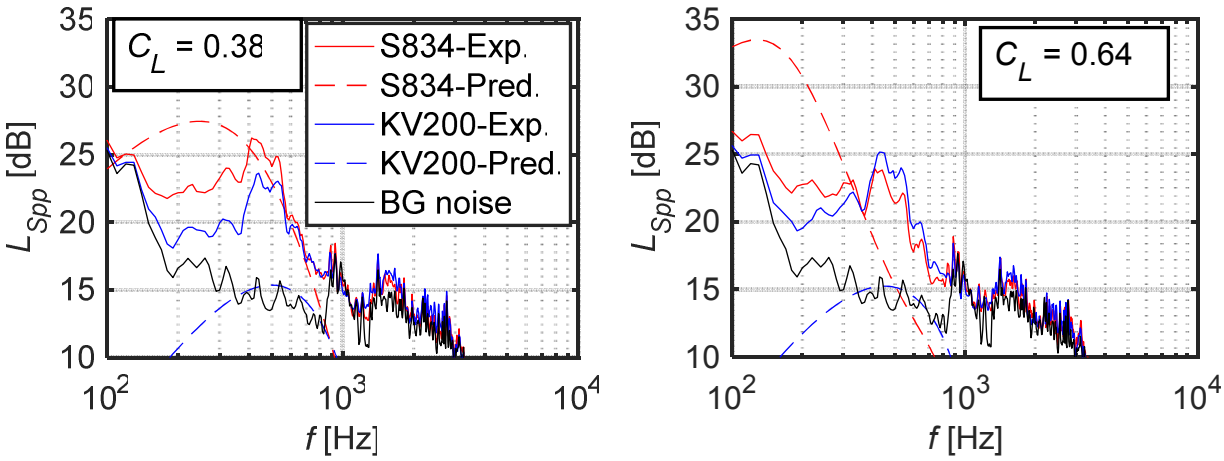

Fig. 4: Measured and predicted far field sound (the black lines indicate the empty wind tunnel measured background (BG) noise)

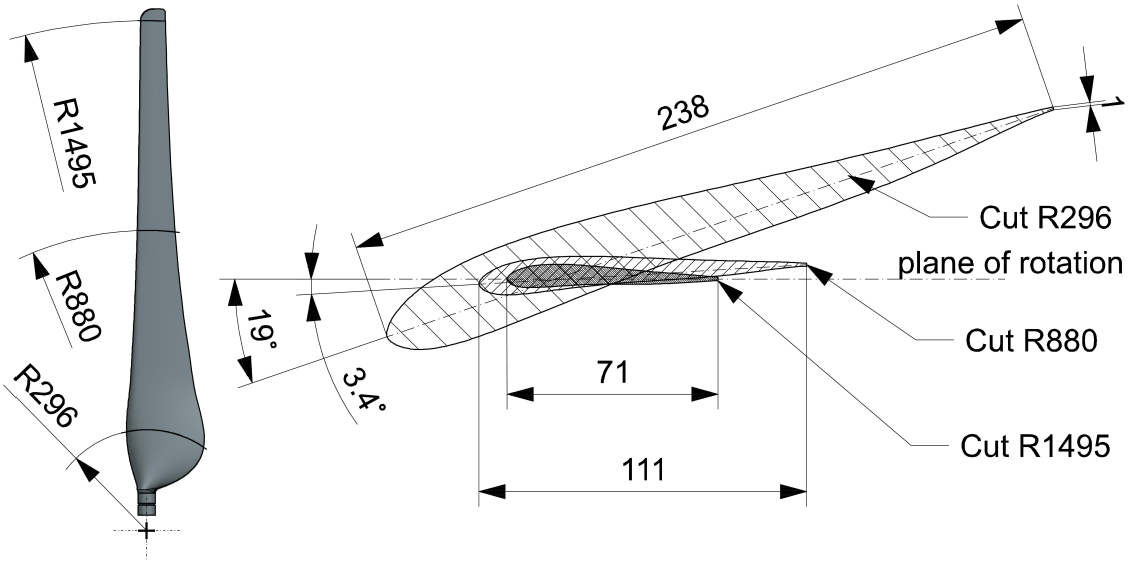

Fig. 5: Contour and section views of the new blade B-KV200

Two half shells were manufactured from carbon fibre reinforced raisin in a 3D milled mold, Fig. 6, and glued together. Special attention was given to thickness of the trailing edge. As compared to the baseline blade it was reduced from 1.5 mm ± 0.1 mm to 1 mm ± 0.1 mm. The purpose was to keep the ratio of trailing edge thickness to displacement thickness h/δ^* and hence the possible bluntness noise low (this is guided by the BPM-model [27], appendix E).

Fig. 6: The two halfs of the mold and the new blade B-KV200

3.3 Experimental turbine performance validation

As suspected from the description in appendix A the University of Siegen wind turbine test site is a low wind speed site in a non-ideal urban environment. The terrain is non-flat. The site is located at a large flat roof of the tallest building in the area, but, depending on the wind direction, with the potential of vortices developing on the roof edges. This requires measurements over several days or even months and a statistical analysis of all experimental data.

A prerequisite for a fair comparison of the baseline and the acoustically optimized turbine is that the power output of both turbines is similar. Fig. 7 (left) demonstrates that - although the measurements from both turbines were taken at different times - the probability distributions of the turbulent intensity are very similar. The turbulent intensity of the wind speed is

$$TI = \sigma_{ceff} / c_{eff} \tag{13}$$

with the standard deviation of the effective wind speed σ_{ceff}. Hence, TI is regarded as equivalent for both measurement campaigns. Fortunately, also the shaft power distribution of both turbines turned out to be very similar as seen in Fig. 7 (right). This means that the new blades B-KV200 are aerodynamically more or less equivalent.

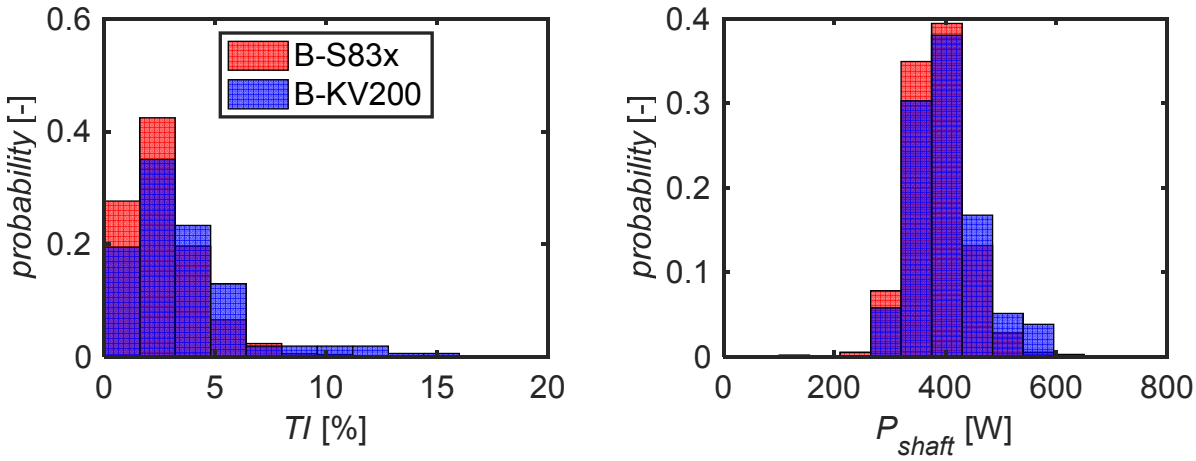

Fig. 7: Probability distributions of recorded 1 s time frames, left: turbulent intensity of upstream wind, right: turbine shaft power

The median sound pressure spectrum from both turbines from the off- and on-axis turbine mounted microphone is shown in Fig. 8. It should be noted that the spectra for the new blade appears less smooth as the number of available time windows utilized to build the median spectra was considerably smaller. The signal-to-noise ratio is superb. After all, the new blade design offers a noise reduction of up to 4 dB in the psychoacoustically important frequency band between 1000 and 4000 Hz. This is also clearly audible. Note that in this frequency range TE noise is expected considering the BPM-model (appendix E). The frequencies are higher compared to the wind tunnel measurements as the chord length of the blade is much smaller while the Reynolds number is the same. On the other hand a significant increase of noise is found towards higher frequencies. An explanation for this increase cannot be given yet.

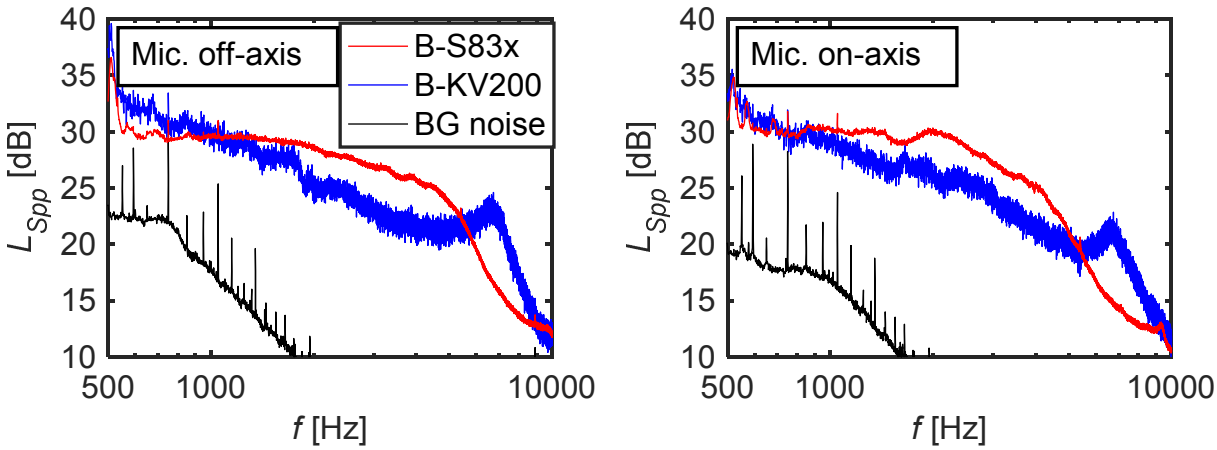

Fig. 8: Sound pressure at off- and on-axis turbine mounted microphone: Median power spectral density from baseline and new blade; BG = background noise

4. Summary and conclusions

The aerodynamic noise of a small wind turbine, originally equipped with NREL's S83x airfoil shaped blades, could be reduced by up to 4 dB in the frequency range from 1 to 6 kHz. The penalty is an increase of high frequency noise at around 7.5 kHz. An explanation for this increase cannot be given yet, in particular, since the wind tunnel measurements with the airfoil segment do not show this behaviour (even without tripping (not shown here)). Tip noise is not expected as the lift distribution is kept the same compared to the baseline turbine. Additionally, the frequency is too high for bluntness noise to be expected (appendix E). One has to keep in mind that the wind turbine blades - in contrast to the blade elements in the wind tunnel - are not tripped. Laminar effects could produce this excessive sound. The modification of the turbine's noise signature is clearly audible close to the turbine. In the distance of less than 100 m a listener does not perceive the high frequency component and experiences a substantial reduction of the turbine noise. The control of the turbine is such that in average it operates at design tip speed ratio (λ = 7.5). Off-design points are not considered in this study. The overall aerodynamic performance of the new blades is equivalent or even slightly better than the baseline.

This progress had been achieved by a new aeroacoustically optimized airfoil shape. By integrating a combined KAMRUZZAMAN/AMIET trailing edge noise prediction model into an evolutionary algorithm, a new airfoil shape was identified. Key idea was to "design" the turbulent boundary layer close to the trailing edge such that it promises lowest trailing edge sound. Despite the relatively poor performance of the semi-empirical (but computationally not costly) trailing edge sound prediction model, wind tunnel tests at a Reynolds number of 200,000 confirmed that the new airfoil produces less self-noise than the benchmark.

Acknowledgment

The authors thank Julien Christophe from the von Kármán Institute for Fluid Dynamics in Sint-Genesius-Rode, Belgium for discussions regarding AMIET's theory and supplying a code with AMIET's trailing edge noise model. Moreover, we gratefully appreciate the assistance by Dipl.-Ing. B. Homrighausen and Mr. J. Graf for designing the mold and manufacturing the blades.

Appendix A: The University of Siegen wind turbine test site

The University of Siegen wind turbine test site is located at a large flat roof of the tallest building in the area, but, depending on the wind direction, with the potential of vortices developing on the roof edges. The wind turbine to be tested is equipped with and surrounded by several sensors, Fig. A1:

- three wind speed cup anemometers
- three wind direction sensors
- rotational speed sensor
- voltage and current sensors
- rain sensor
- two permanent, weatherproof microphones (Microtech Gefell WME 952)

Fig. A1: Wind turbine and measurement stations M1, M2 and M3; each station is equipped with a cup anemometer and a wind vane type wind direction sensor

Cup anemometers and wind direction sensors are mounted on three stations positioned on a circle with a radius of 2.5 turbine diameters around the turbine (cp. IEC 61400-12-1 [29]) abreast of the nacelle. The effective wind speed c_{eff} relevant for the turbine is determined by spatially averaging all anemometer signals which are not in the wake of the turbine. The wake is assumed to cover a 74° cone (cp. IEC 61400-12-1 [29]) downstream of the turbine.

The positions of the two turbine mounted microphones are depicted in Fig. A2. The purpose of attaching the microphones to the permanently yawing turbine is to measure the sound always in well-defined positions relative to the turbine rotor. The possible draw back is that vibrations from the structure may contaminate the microphone signals. A separate study proved that this is irrelevant.

Within a special campaign, a microphone array consisting of 40 microphones irregularly located on an area of 0.75 m^2 (CAE Noise Inspector™) can be mounted on the wind turbine nacelle downstream of the rotor and even the wind vane, the center of the array being close to the rotational axis of the turbine. Standard beam forming is used for post-processing.

Data of all sensors - excluding the microphones - are sampled and saved to hard disc continuously 24 hours per day with a sampling rate of 10 Hz. Microphone data sampling with 40 kHz is only triggered when the wind speed is in an interesting range in order to save disc space. Data aquisition and storage is managed via an inhouse Labview™ based code.

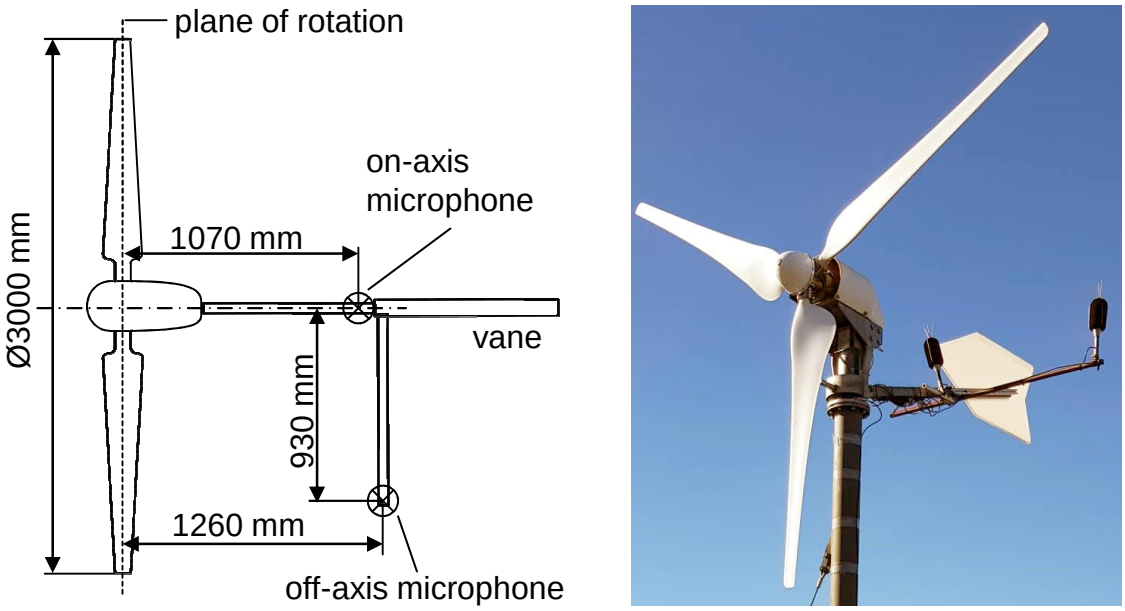

Fig. A2: Turbine mounted microphones (on-axis and one off-axis), left: schematic top-view diagram (not to scale)

As this roof-mounted wind turbine faces a rather dynamic wind speed it was decided to evaluate short time data windows of 1 s. To compensate for scatter of data through the dynamic wind speed and the time delay between measured wind speed and turbine speed, statistical methods are applied for evaluation. A 1 s window is as assigned "valid" if it satisfies following conditions:

1. The arithmetically averaged wind speed is in a range of ±1% of the design wind speed (6 m/s)
2. The arithmetically averaged tip speed ratio is in a range of ±1% of the chosen design tip speed ratio (7.5)
3. The electrical power is > 50 W in order to exclude recordings where the turbine was not yet feeding power into the grid (idling)
4. No precipitation (rain or snow)

Non-acoustic data are arithmetically averaged for each time window. The turbine shaft power P_{shaft} is derived from the calibrated electric generator power.

The acoustic data can be contaminated by background noise from the environment (road, train traffic etc.). Hence, for each valid time window a spectrum is evaluated. The resulting set of spectra are then reduced to one median spectrum. The median is insensitive against outliers (HANSEN et al. [30]). For evaluating the signal-to-noise ratio of the acoustic turbine signature, the background noise is evaluated in the same way but with the turbine stopped.

Appendix B: Prestudy: Detection of noise sources of the baseline wind turbine

Detection of noise sources via microphone array

Fig. B1 shows the acoustic map during operation of the turbine at around design wind speed. It can be seen that the outer span but not the tip of the turbine is the

main noise source. As the microphone array (CAE Noise Inspector™) is mounted with its centre close to the axis, a rotationally symmetric acoustic picture would be expected, i.e. the acoustic picture should resemble a red donut. In contrast just the right side of the turbine on the picture in Fig. B1 is highlighted. A non-symmetrical distribution of the individual array microphones off the axis is thought to be the reason. However, the dominant noise source is still proved to be the outer blade region but not the tip.

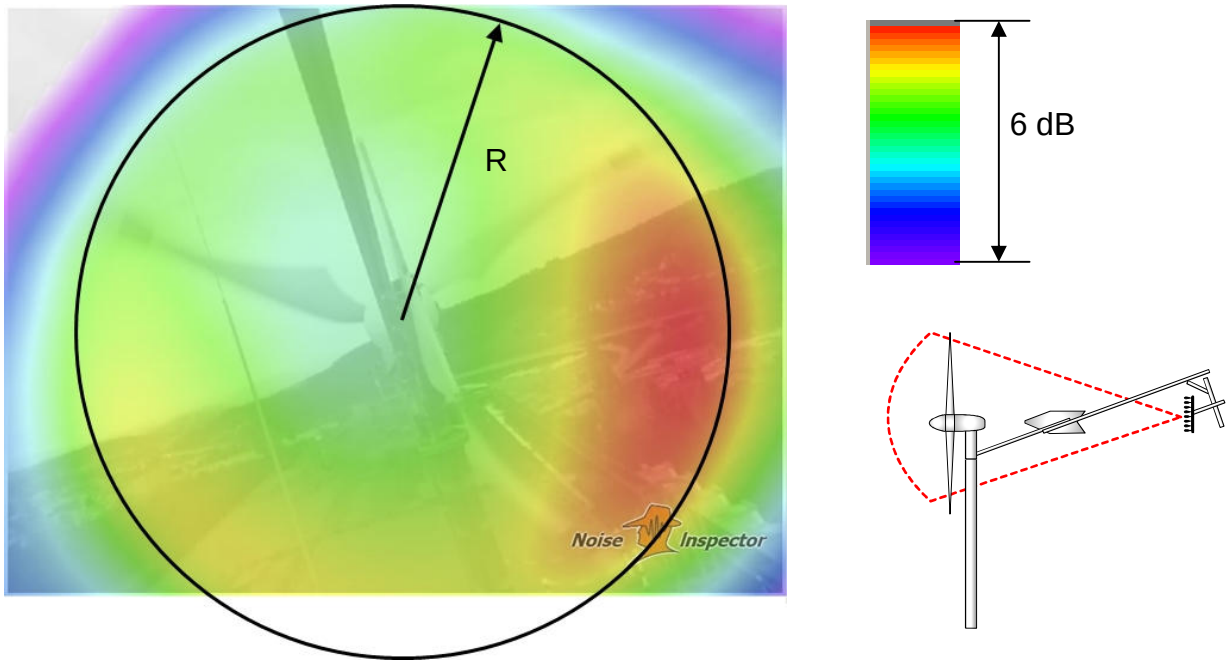

Fig. B1: Sound pressure map for the frequency range 630 - 10000 Hz. Lower right: Microphone array mounted downstream of the wind vane, the red frame shows the field of observation of the microphone array

Detection of noise sources via amplitude modulation

For our purpose the evidence of amplitude modulation can prove the blades to be the dominant noise source. Amplitude modulation is defined as the periodic varying noise levels a microphone receives under following conditions: a) the dominant noise source are the rotating blades and b) the microphone is located off-axis (rotational axis). The frequency of the variation is the blade passing frequency of the turbine. For the here considered small wind turbine it is around 15 Hz under design operating conditions. Those facts can be used to detect if blade noise is the dominant noise source in chosen frequency bands of the recorded noise spectrum. Here we slightly modify the method for evaluation of amplitude rating from the IOA Noise Working Group (BASS et al. [31]) to consider the higher blade passing frequency of the small baseline wind turbine:

A subset of 60 1 s time windows (instead of 100 10 s windows in the original IOA method)

1. Each time frame is band pass filtered to search for the occurrence of amplitude modulation in this frequency band (here: 1/3rd-octave bands instead of the fewer frequency bands in the original method)

2. Each band pass filtered time frame is subdivided into 1 ms intervals (instead of 100 ms in the original method)
3. Calculation of overall sound pressure level for each 1 ms time signal
4. Search for amplitude modulation occurring with blade passing frequency following the procedure of the IOA method
5. If in 50% or more of the 60 time frames occurrences of amplitude modulation are found in the noise records, amplitude modulation is proven according to the methodology.

Fig. B2 shows the found amplitude ratings for the whole spectrum in the recordings of the microphone off-axis. The fact that amplitude modulation was found for frequencies larger than 500 Hz proofs that the dominant noise source in the acoustic records has to be blade noise in these frequencies. For frequencies of 500 Hz or lower no amplitude modulation can be found indicating that other noise sources (e.g. vibrations or electrical generator) are dominant.

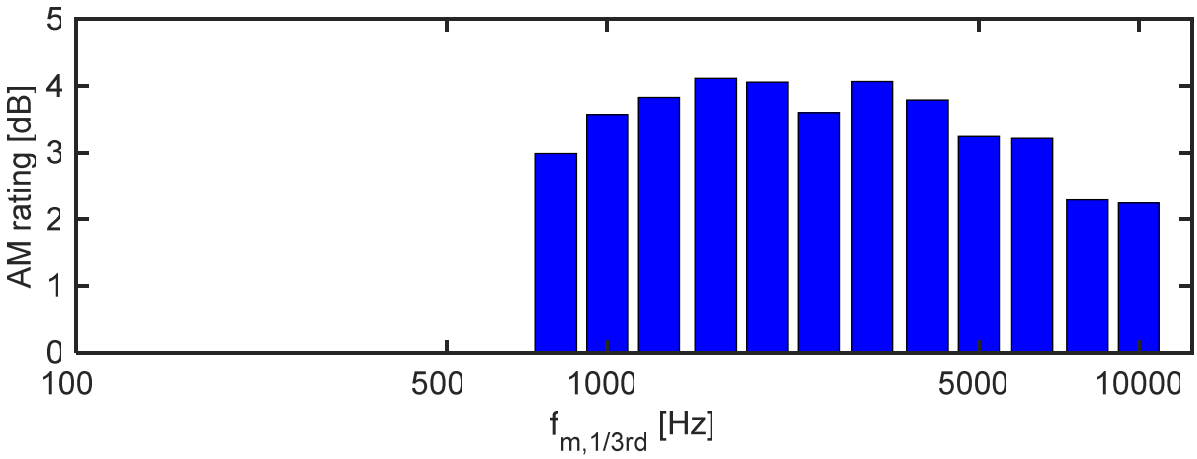

Fig. B2: Occurrence of amplitude modulation found in the noise spectrum of the microphone off-axis

Appendix C: Experimental wind tunnel setup

The aeroacoustic wind tunnel of the University of Siegen is schematically depicted in Fig. C1. It is designed to test airfoil sections with a chord length *C* of 200 mm and a span *L* of 266 mm. The airfoil sections are vertically mounted between side plates and 0.5 *C* in front of the nozzle exit.

Since the airfoil section is placed into a jet flow and not in a free flow, the geometric angle of attack used for mounting the airfoil section is not equal to the effective angle of attack α the airfoil experiences. Hence, for mounting the airfoil section an angle of attack correction by BROOKS [32] is utilized and checked via a comparison of the streamwise pressure distributions form measurements and a *XFOIL*-prediction [20].

The far field noise is measured with 12 microphones (1/2" Brüel & Kjaer™, type 4190) aligned on a sector of a circle with 0.5 m radius around the trailing edge (depicted in Fig. C2). Here we consider only the noise at microphone M10 on the pressure side is evaluated as it offers a high signal to background noise ratio. Jet shear layer diffraction errors were neglected because of the low flow velocities.

Time signals of far field microphones are captured for 30 s. The signal analysis is based on the power spectral density which was obtained by the function *pwelch* in MATLAB™ Vers. 9.1. The parameters chosen for *pwelch* are a *Hanning* window, the overlap between sections is 0.5 (MATLAB standard) and the number of discrete Fourier points (*nfft*) is equal to the section length. The spectra of each section is averaged to obtain the final spectrum with a frequency resolution of Δf = 10 Hz.

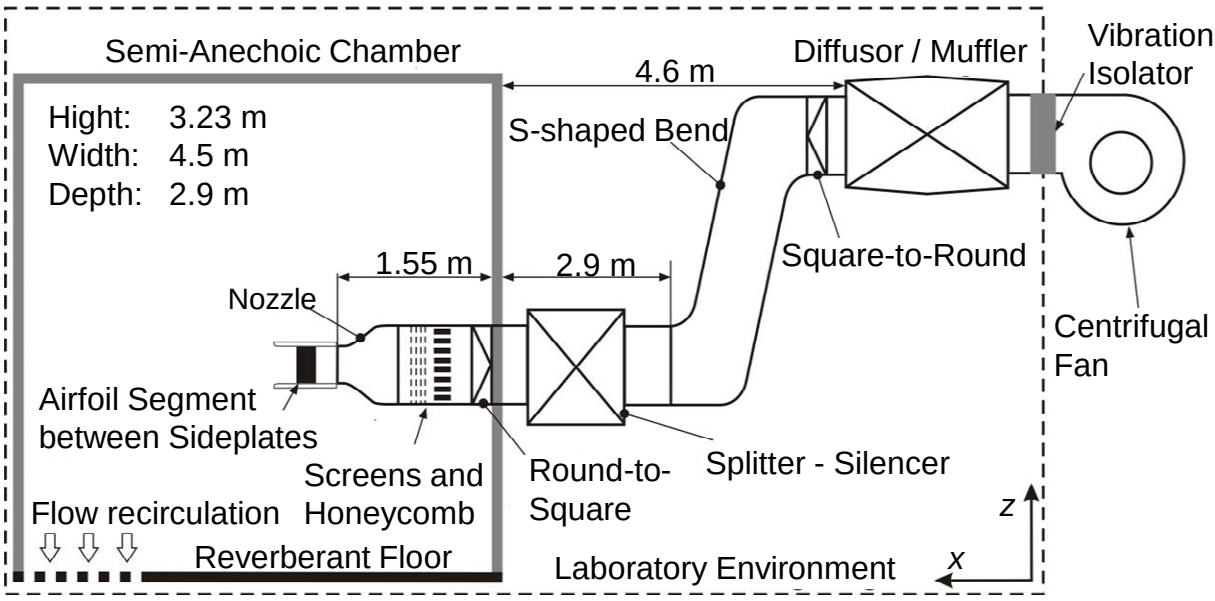

Fig. C1: Schematic layout of the aero-acoustic wind tunnel (not to scale)

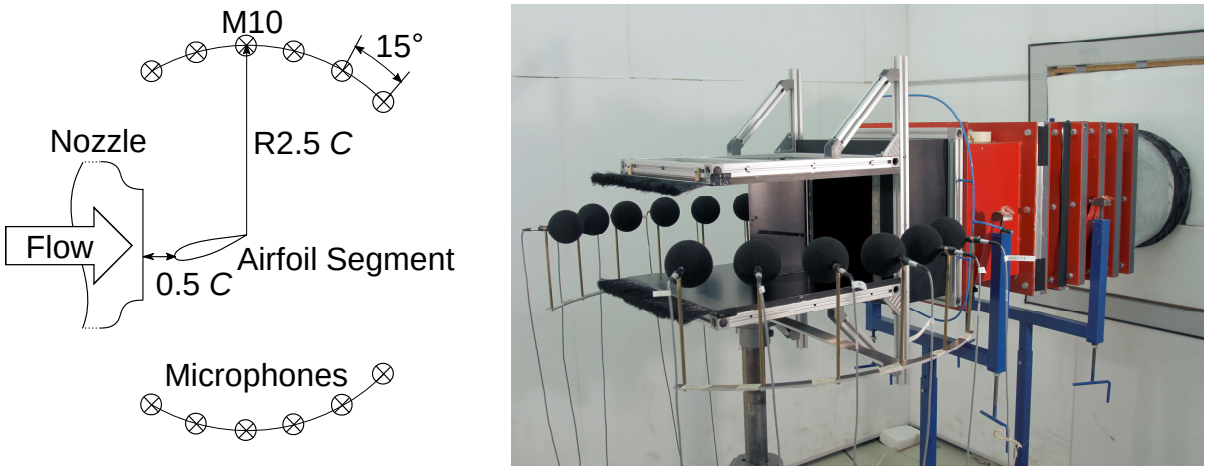

Fig. C2: Left: Schematic diagram of microphones around airfoil section (not to scale); right: Test rig and microphones in semi anechoic chamber

Appendix D: Definition of averages and levels

The power spectral density of the far field sound pressure S_{pp} calculated with eq. (6) can be written in terms of a level

$$L_{Spp} = 10\log_{10}\left(\frac{S_{pp}\cdot\Delta f_{ref}}{p_{ref}^2}\right) \quad \text{dB} \tag{D1}$$

with the reference sound pressure p_{ref} = 2·10^{-5} Pa and the reference frequency bandwidth Δf_{ref} = 1 Hz. Integration of the power spectral density of the wall pressure fluctuations and far field sound pressure, here over the frequency range 100 Hz to 10 kHz, yields the overall far field sound pressure level *OSPL*

$$OSPL = 10\log_{10}\left(\frac{\int_{100\text{ Hz}}^{10000\text{ Hz}} S_{pp}(f)\,df}{p_{ref}^2}\right) \quad \text{dB}. \tag{D2}$$

The predicted power spectral density of the far field sound pressure S_{pp} is a function of frequency *f*, chordwise position ξ (that is used for the prediction of the wall pressure fluctuations) and the angle of attack α of the airfoil section. AMIET's model predicts the far field sound based on pressure fluctuations at one single chordwise position. Usually, this chordwise position is chosen to be *close to* the trailing edge but not exactly at the trailing edge. There is no accepted rule for choosing this position. Moreover, performing an optimization, based on one single chordwise position, would lead to a very local modification of the airfoil shape. Moreover, the sound pressure level for a complete range of angle of attacks shall be reduced. Therefore, a spatially (in stream or chordwise direction) and for a range of angle of attacks averaged overall far field sound pressure level is utilized. Averaging is done over *n* chordwise positions between 80% *C* to 98% *C* and *m effective* angles of attack between 2° and 6°:

$$\overline{\overline{OSPL}}_{obj} = 10\log_{10}\left(\frac{\frac{1}{m}\sum_{i=1}^{m}\left[\frac{1}{n}\sum_{j=1}^{n}\left[\int_{100\text{ Hz}}^{10000\text{ Hz}} S_{pp}\left(f,\xi_j,\alpha_i\right)df\right]\right]}{p_{ref}^2}\right) \tag{D3}$$

Appendix E: An estimate of trailing edge and trailing edge bluntness noise frequencies

A first estimate of the characteristic frequencies for trailing edge and trailing edge bluntness noise is obtained via the BROOKS-POPE-MARCOLINI (BPM) model [27] There, the spectral peak is at a Strouhal number value

$$St_{peak} = \frac{ls\cdot f_{peak}}{w_\infty} = 0.1, \tag{E1}$$

where f_{peak} is the peak frequency and *ls* a characteristic length scale. The length scale is either the boundary layer displacement thickness δ^* for trailing edge noise or the trailing edge thickness *h* for the trailing edge bluntness noise.

Within the wind turbine application the blade section at spanwise position r/R = 0.9 is considered to be the most dominant regarding noise emission. For a lift coefficient C_L = 0.64 (according to lift distribution on wind turbine) for both, the S834 and the KV200 airfoil shape at Re = 200,000, XFoil by DRELA [20] is utilized to predict the displacement thickness on the suction side. With these inputs the expected characteristic peak frequencies can be determined, Tab. E.

Tab. E: Predicted peak frequencies for blade sections according to the BPM-model

	Airfoil segment for wind tunnel test		Wind turbine	
	S834	KV200	S834	KV200
C	200 mm		80 mm	
h	0.4 mm		1.5 mm	1.0 mm
δ^* (XFoil predicted)	6.3 mm	2.4 mm	2.5 mm	1.0 mm
h/δ^*	0.06	0.16	0.6	1.0
f_{peak} (TE noise)	230 Hz	600 Hz	1600 Hz	4200 Hz
f_{peak} (TE bluntness noise)	3700 Hz		2700 Hz	4100 Hz

The predicted spectral peak of trailing edge noise is well within the dominant frequencies in wind tunnel and wind turbine measurements, and of trailing edge bluntness noise (if present) well within the dominant frequencies of the wind turbine measurements (while hidden in the background noise in the wind tunnel measurements (if present). According to the BPM-model bluntness noise is only relevant for a relative thickness of the trailing edge h/δ^* > 0.3. Hence, bluntness noise is not expected to be present at the wind tunnel tests but might be present at the wind turbine measurements. The trailing edge thickness of the new blade was reduced in order to keep h/δ^*. Indeed, there is no indication of bluntness noise in the turbine's acoustic signature (Fig. 8).

The airfoil optimization considered the worst-case scenario of fully turbulent boundary layers. However, the position of laminar to turbulent transition on the turbine blades is not fixed with tripping but natural. This has an effect on the predicted displacement thickness and, hence, both noise mechanisms. To evaluate this effect, the displacement thickness can also be predicted via XFoil when utilizing a *ncrit* (critical N-factor) of 1 instead of the here applied full-tripping. Essentially, this corresponds to natural transition. The effect on the predicted displacement thickness is insignificant (values not shown here) as compared to the effect of the geometrical airfoil shape.

References

[1] Gerhard, T., Sturm, M., Carolus, T. H.: Small Horizontal Axis Wind Turbine: Analytical Blade Design and Comparison With RANS-Prediction and First Experimental Data. Proceedings of the ASME Turbo Expo 2013

[2] Somers, D. M.: The S833, S834, and S835 Airfoils, National Renewable Energy Laboratory Report No. NREL/SR-500-36340, Golden, Colorado, USA 2005

[3] Howe, M. S.: Noise produced by a sawtooth trailing edge. The Journal of the Acoustical Society of America Vol. 90 (1991) No. 1, p. 482

[4] Gruber, M.: Airfoil noise reduction by edge treatments, Dissertation, Institute of Sound and Vibration Research, University of Southampton, 2012

[5] Klemme, T., Matthias, C. Rotorblatt, Windernergieanlage, Verfahren zum Herstellen eines Rotorblatts und zum Aufstellen einer Windenergieanlage, Offenlegungsschrift, DE102015012428A1, Senvion GmbH, 22297 Hamburg, DE, 25.09.2015, Deutschland

[6] Gerhard, T.: Umströmte Tragflügelsegmente: Auswirkungen des Hinterkantenausblasens auf Strömungsgrenzschicht und Schallemission, Ph.D. dissertation at the University of Siegen. Aachen, Shaker Verlag, 2016

[7] Wolf, A., Lutz, T., Würz, W., Krämer, E., Stalnov, O., Seifert, A.: Trailing Edge Noise Reduction of Wind Turbine Blades by Active Flow Control. Wind Energy Vol. 18 (2015) No. 5, p. 909–923

[8] Lutz, T., Herrig, A., Würz, W., Kamruzzaman, M., Krämer, E.: Design and Wind-Tunnel Verification of Low-Noise Airfoils for Wind Turbines. AIAA Journal Vol. 45 (2007) No. 4, p. 779–785

[9] Oerlemans, S., Schepers, J. G., Guidati, G., Wagner, S.: Experimental demonstration of wind turbine noise reduction through optimized airfoil shape and trailing-edge serrations - NLR-TP-2001-324, Nationaal Lucht- en Ruimtevaartlaboratorium (Ed.), National Aerospace Laboratory NLR, 2001

[10] Amiet, R. K.: Noise due to turbulent flow past a trailing edge. Journal of Sound and Vibration Vol. 47 (1976) No. 3, p. 387–393

[11] Roger, M., Moreau, S.: Back-scattering correction and further extensions of Amiet's trailing-edge noise model. Part 1 - Theory. Journal of Sound and Vibration Vol. 286 (2005) No. 3, p. 477–506

[12] Rozenberg, Y., Robert, G., Moreau, S.: Wall-Pressure Spectral Model Including the Adverse Pressure Gradient Effects. AIAA Journal Vol. 50 (2012) No. 10, p. 2168–2179

[13] Catlett, M. R., Forest, J., Anderson, J. M., Stewart, D.: Empirical Spectral Model of Surface Pressure Fluctuations beneath Adverse Pressure Gradients. 20th AIAA/CEAS Aeroacoustics Conference. 2014

[14] Catlett, M. R., Anderson, J. M., Forest, J. B., Stewart, D. O.: Empirical Modeling of Pressure Spectra in Adverse Pressure Gradient Turbulent Boundary Layers. AIAA Journal Vol. 54 (2016) No. 2, p. 569–587

[15] Hu, N., Herr, M.: Characteristics of Wall Pressure Fluctuations for a Flat Plate Turbulent Boundary Layer with Pressure Gradients. 22nd AIAA/CEAS Aeroacoustics Conference

[16] Kamruzzaman, M., Bekiropoulos, D., Lutz, T., Würz, W., Krämer, E.: A semi-empirical surface pressure spectrum model for airfoil trailing-edge noise prediction. International Journal of Aeroacoustics Vol. 14 (2015) No. 5-6, p. 833–882

[17] Lee, S., Villaescusa, A.: Comparison and Assessment of Recent Empirical Models for Turbulent Boundary Layer Wall Pressure Spectrum. 23rd AIAA/CEAS Aeroacoustics Conference. 2017
[18] Tian, Y., Cotté, B., Chaigne, A.: Wind Turbine Noise Modelling Based on Amiet's Theory. 5th International Meeting on Wind Turbine Noise. 2013
[19] Corcos, G. M.: Resolution of Pressure in Turbulence. The Journal of the Acoustical Society of America Vol. 35 (1963) No. 2, p. 192–199
[20] Drela, M.: XFOIL: An Analysis and Design System for Low Reynolds Number Airfoils. In: Mueller, T. J. (Ed.): Low Reynolds Number Aerodynamics. Proceedings of the Conference Notre Dame, Indiana, USA, 5-7 June 1989. Lecture Notes in Engineering, Vols.54. Berlin, Heidelberg: Springer 1989, p. 1–12
[21] Kaufmann, N.: Optimierung des hydrodynamischen Entwurfs einer Gezeitenströmungsturbine, Diplomarbeit, Lehrstuhl für Strömungsmechanik und Strömungsmaschinen, Technische Universität Kaiserslautern, 2015
[22] Bamberger, K.: Aerodynamic Optimization of Low-Pressure Axial Fans. Berichte aus der Strömungstechnik, Ph.D. dissertation at the University of Siegen. Herzogenrath, Shaker, 2015
[23] Thévenin, D., Janiga, G.: Optimization and Computational Fluid Dynamics. Heidelberg, Germany, Springer Verlag GmbH, 2008
[24] Giguere, P., Selig, M. S.: New Airfoils for Small Horizontal Axis Wind Turbines. Journal of Solar Energy Engineering (1998) No. 120(2), p. 108–114
[25] Clauser, F. H.: Turbulent Boundary Layers in Adverse Pressure Gradients. Journal of the Aeronautical Sciences Vol. 21 (1954) No. 2, p. 91–108
[26] McAuliffe, B. R., Yaras, M. I.: Transition Mechanisms in Separation Bubbles Under Low- and Elevated-Freestream Turbulence. Journal of Turbomachinery Vol. 132 (2010) No. 1, p. 11004
[27] Brooks, T. F., Pope, D. S., Marcolini, M. A.: Airfoil Self-Noise and Prediction, NASA Reference Publication 1218 (Ed.), NASA Langley Research Center, 1989
[28] Schepers, J. G., Wuerz, W., Curvers, A., Mantesanz, A., Oerlemans S., Garcillan, L., Braun, K., Fischer, M., Lutz, T., Koegler, K., Herrig, A., Maeder, T.: SIROCCO: Silent rotors by acoustic optimisation, ECN Energy research Centre of the Netherlands, 2007
[29] IEC 61400-12-1:2017. Wind energy generation systems - Part 12-1: Power performance measurements of electricity producing wind turbines. [online]: https://webstore.iec.ch/publication/26603
[30] Hansen, C. H., Doolan, C. J., Hansen, K. L.: Wind farm noise - Measurement, assessment and control. Wiley series in acoustics, noise and vibration. Hoboken, John Wiley & Sons Inc, 2017
[31] Bass, J., Cand, M., Coles, D., Irvine, G., Leventhall, G., Levet, T., Miller, S., Sexton, D., Shelton, J.: A Method for Rating Amplitude Modulation in Wind Turbine Noise - IOA Noise Working Group (Wind Turbine Noise), Amplitude Modulation Working Group, Final Report, INSTITUTE OF ACOUSTICS, 2016 (Version 1. Auflage)
[32] Brooks, T. F., Marcolini, M. A., Pope, D. S.: Airfoil Trailing-Edge Flow Measurements. AIAA Journal Vol. 24 (1986) No. 8, p. 1245–1251